Tellus
SINCE 1948

COLLECTION: TELLUS 75TH JUBILEE SPECIAL COLLECTION: CELEBRATING LEGACY AND SHAPING THE FUTURE OF EARTH SYSTEM SCIENCE

PERSPECTIVE

# A New Method for Characterising Carbon Cycle Sensitivities in Earth System Models

**PETER M. COX**
**JOSEPH J. CLARKE**
**SIMON R. G. JONES**
**REBECCA M. VARNEY**

*Author affiliations can be found in the back matter of this article

STOCKHOLM UNIVERSITY PRESS

## ABSTRACT

Carbon cycle feedbacks play a key role in past climate variations and may also have a significant impact on future climate. However, it was not until the early 2000s that general circulation models (GCMs) of the climate started to include carbon cycle feedbacks on climate change. The results of the first two climate-carbon GCMs were compared in a paper published in *Tellus*. Following those first model runs, many other such 'Earth System Models (ESMs)' have been developed and compared as part of the Coupled Climate-Carbon Cycle Model Intercomparison project ($C^4$MIP). Modelled changes in global land and ocean carbon storage have been routinely compared using a simple formalism that assumes a linear dependence of global land and ocean carbon storage on both atmospheric $CO_2$ increase and global warming. This $\beta$-$\gamma$ formulation has been very helpful to identify the zeroth-order reasons for differences between ESM projections, but it is unable to reproduce the saturating time-evolution of global land and ocean carbon storage as simulated by the $C^4$MIP models. In this paper, we summarise work to date on modelling the coupled climate-carbon cycle system, and suggest an update to the $\beta$–$\gamma$ formulation to include a representation of sink saturation as well as the timescale dependencies of land and ocean carbon uptake. Our new approach adds half-saturation constants, $\kappa$, for quasi-equilibrium land and ocean carbon increases with $CO_2$, and land and ocean timescales, $\tau$, that approximate how quickly this quasi-equilibrium is approached. This new '$\beta$–$\gamma$–$\kappa$–$\tau$' formulation reproduces the $C^4$MIP results with much greater accuracy than the existing $\beta$–$\gamma$ formulation, without requiring any additional ESM runs to be analysed.

**CORRESPONDING AUTHOR:**
**Peter M. Cox**
Faculty of Environment, Science and Economy, University of Exeter, Exeter, UK; Global Systems Institute, University of Exeter, Exeter, UK
p.m.cox@exeter.ac.uk

**KEYWORDS:**
Climate Change; carbon fluxes; Earth system model

**TO CITE THIS ARTICLE:**
Cox, P. M., Clarke, J. J., Jones, S. R. G., & Varney, R. M. (2026). A New Method for Characterising Carbon Cycle Sensitivities in Earth System Models. *Tellus*, 79(1): 173–187. DOI: https://doi.org/10.16993/tellus.4128

## 1 INTRODUCTION

Since the pioneering work of Keeling (1960), published in *Tellus*, it has been well established that the concentration of atmospheric $CO_2$ has been increasing rapidly since the start of the Industrial Revolution, which has in turn led to a rise in global average temperatures. The growth of $CO_2$ is due to human activity, primarily the burning of fossil fuels, but with a significant contribution also from deforestation and other land-use change. As global populations, economies, and industries have expanded, their increasing energy and material demands have resulted in anthropogenic $CO_2$ emissions that increased almost exponentially over the past 200 years. However, the atmospheric $CO_2$ concentration has only increased by less than half of the anthropogenic emissions (Friedlingstein et al., 2024). This discrepancy is the result of significant natural carbon sinks on the land and in the ocean (Bolin, 1977; Bolin et al., 1989; Revelle and Suess, 1957).

However, land and ocean carbon sinks are not static. Terrestrial and marine carbon uptake varies over seasonal to millennial time-scales, and the magnitude of these variations depends on the responses of physical and biological processes to changes in both atmospheric composition and physical climate. These responses can either slow or accelerate the rate of climate change, leading to 'climate-carbon cycle feedbacks' which are a key source of uncertainty in future projections (Friedlingstein et al., 2014). The role of climate-carbon cycle feedbacks is also very evident in past climate variations. Most notably, during glacial–interglacial periods, changes in $CO_2$ drive a significant part of the glacial–interglacial changes in temperature (Petit et al., 1999; Sigman and Boyle, 2000).

The gross uptake of carbon by land and ocean depends on the concentration of $CO_2$ in the atmosphere. Terrestrial ecosystems sequester $CO_2$ through photosynthesis, which is stimulated by increased atmospheric $CO_2$ if nutrients are also available (Walker et al., 2021). Similarly, diffusion of $CO_2$ from the atmosphere into the surface layer of the ocean is controlled by the difference in partial pressures ($pCO_2$) between the ocean and atmosphere. As a result, since the start of the industrial revolution, land and ocean sinks have kept pace with the near-exponential increase in anthropogenic emissions, evidenced by the long-term stability of the airborne fraction of $CO_2$ emissions (Friedlingstein et al., 2024; Jones and Friedlingstein, 2020). However, the fraction of anthropogenic emissions removed by land and ocean carbon sinks is projected to decrease under climate change (Canadell et al., 2021).

On the land, $CO_2$ fertilisation relies heavily on sufficient nutrient supply, which, despite large anthropogenic production of reactive nitrogen (Zhu et al., 2025), is not always available (LeBauer and Treseder, 2008). Nutrient cycles in some areas remain relatively closed. Old-growth tropical forests, for example, are typically limited by phosphorus (Walker and Syers, 1976), which restricts their potential $CO_2$ uptake in the future. Changes in climate may also take plants outside their natural ranges. In the ocean, rising sea surface temperatures and increasing dissolved inorganic carbon (DIC) concentrations reduce the rate of $CO_2$ uptake (Egleston et al., 2010; Revelle and Suess, 1957). These effects contribute to 'sink saturation' and declining sink efficiency under increasing $CO_2$, which may reduce carbon uptake and accelerate global climate change in the future (Canadell et al., 2021).

Nevertheless, it was not until the early years of this millennium that general circulation models (GCMs) of the climate began to include interactions between the climate and carbon cycle (Cox et al., 2000; Friedlingstein et al., 2001). Indeed, *Tellus* published an intercomparison of the first two climate-carbon cycle GCMs in 2003 (Friedlingstein et al., 2003). These models were the forerunners of what are now called 'Earth System Models (ESMs)', and ultimately led to the 'Coupled Climate-Carbon Cycle Model Intercomparison Project ($C^4$MIP)' (Arora et al., 2013, 2020; Friedlingstein et al., 2006). $C^4$MIP compares results from multiple ESMs using a quasi-equilibrium linear formulation that was first proposed in that 2003 paper in Tellus. This '$\beta$–$\gamma$' formulation has the advantage of being very simple to use, but is unable to capture vital aspects of sink saturation.

This paper for the *Tellus 75^th^ Anniversary* issue aims to summarise work on coupled-climate carbon cycle modelling (Section 2), and also to propose a long-overdue update to the '$\beta$–$\gamma$' characterisation of carbon cycle sensitivities to $CO_2$ and climate, to capture sink saturation effects (Section 3).

## 2 THE EVOLUTION OF COUPLED CLIMATE-CARBON CYCLE MODELS

As described above, the importance of climate-carbon interactions had been revealed throughout the last 30 years of the 20th century. Although 'full-form' GCMs were beginning to include coupling between the climate and the ocean carbon cycle on long timescales (Sarmiento and Toggweiler, 1984), these had not yet included the land carbon cycle. GCM land surface schemes, which had traditionally focused on calculating land-atmosphere fluxes of energy, water, and momentum, were diversifying to also calculate plant photosynthesis (Cox et al., 1999; Sellers et al., 1996a). Initially, this was to improve the simulation of water fluxes over land, which is heavily influenced by stomatal pores on plant leaves (Sellers et al., 1997), by making use of empirical relationships between photosynthesis and stomatal conductance (Ball et al., 1987). These second-generation land surface models therefore coupled the water and carbon fluxes, but still required prescribed fixed maps of vegetation types and land-surface parameters (Pitman, 2003; Sellers et al., 1996b).

In parallel, a separate group of researchers had begun to develop dynamic global vegetation models (DGVMs), with the aim of simulating the changing geographical distribution of vegetation types under climate change (Cramer et al., 2001). These models were derived from biogeographical models developed for palaeoclimate reconstructions (Haxeltine and Prentice, 1996; Prentice et al., 1992), but were also increasingly based on the principles of carbon and water balance (Woodward, 1987). Before the end of the 20th century, a first attempt was made to asynchronously couple a DGVM to a GCM climate model (Betts et al., 1997). However, the pieces were now in place for a GCM of the fully coupled climate-carbon system, which are today referred to as 'ESMs' (Randall et al., 2019).

At the beginning of the 21st century, the first ESMs were published. A group based at the UK Met Office-Hadley Centre developed a variant of the HadCM3 climate model which included representations of the ocean carbon cycle (Palmer and Totterdell, 2001) and land carbon cycle (Cox et al., 1999), and also a simple representation of vegetation dynamics (Cox, 2001). A fully coupled climate-carbon cycle run was compared to a model run with prescribed $CO_2$ concentrations, to isolate the impact of climate-carbon feedbacks on the rate of $CO_2$ increase and global warming. Alarmingly, this study reported that climate-carbon cycle feedbacks increased projected atmospheric $CO_2$ by 270 ppmv, and global warming from 4°C to 5.5°C, by the end of the 21st century (Cox et al., 2000). The acceleration of climate change in this model was primarily due to the suppression of the global land carbon sink by climate change, which ultimately transitioned to a carbon source from about 2050 onwards, due to increased rates of soil respiration and Amazon forest dieback under global warming (Cox et al., 2004).

Independently, a group at the IPSL in France was also developing a climate-carbon cycle model (Friedlingstein et al., 2001), making use of the IPSL-OGCM1 ocean carbon cycle model (Le Quéré et al., 2000) and the SLAVE terrestrial carbon cycle model (Friedlingstein et al., 1995). Under a prescribed 1% per year increase in atmospheric $CO_2$, this model also simulated a suppression of the land carbon sink by climate change, with land carbon uptake at the time of doubling $CO_2$ reduced by about a quarter. These first two ESM simulations (Cox et al., 2000; Friedlingstein et al., 2001) suggested that climate change would suppress natural carbon sinks and therefore provide an amplifying positive feedback on climate change. However, the magnitude of the positive feedback differed markedly in the two models. In order to isolate the reasons for this, a collaborative study was undertaken between the French and UK groups. The resulting paper, published in *Tellus* (Friedlingstein et al., 2003), identified a stronger negative response of the land carbon cycle to climate change in the UK model as the key reason for the differences between them.

Prompted by these initial studies which suggested that carbon cycle feedbacks on future climate could be large but were uncertain, the $C^4$MIP was set up to enable a cleaner comparison between the results from the growing number of coupled climate-carbon cycle models. The first phase of $C^4$MIP used a common emissions scenario (SRES A2) and required global atmospheric $CO_2$ concentration to be simulated internally within each model. All models produced a positive climate-carbon feedback on climate change, but with a range that differed by an order of magnitude from an extra 20 to 200 ppmv of $CO_2$ by 2100 (Friedlingstein et al., 2006). Two further phases of $C^4$MIP have since been carried-out, based, respectively, on the CMIP5 and CMIP6 generations of ESMs (Arora et al., 2013, 2020). These latter $C^4$MIP studies used a simpler experimental design in which the atmospheric $CO_2$ concentration is prescribed to increase at 1% per year, and model runs are carried out with ('COU'; coupled runs) and without ('BGC'; biogeochemical runs) climate effects on the carbon cycle, to separate the direct-$CO_2$ effects (see Figure 1; Jones et al. (2016)). Each generation of $C^4$MIP models has seen further developments. For example, additional nutrient limitations on land and ocean carbon sinks were implemented for CMIP6, and the range of carbon cycle projections has generally been reduced (Canadell et al., 2021). However, significant uncertainty remains, especially in the response of the land carbon cycle, which is also impacted by land-use change (Arora et al., 2020). As a result, methods to separate impacts on the carbon cycle remain important.

### 2.1 STANDARD $\beta$–$\gamma$ DIAGNOSIS OF CARBON CYCLE SENSITIVITIES

To quantify carbon cycle sensitivities within climate-carbon cycle models (ESMs), a standard $\beta$–$\gamma$ framework has been followed since first introduced in Friedlingstein et al. (2003). Carbon cycle sensitivities are defined using two parameters: known as the carbon-concentration sensitivity ($\beta$), quantifying the sensitivity of land and ocean carbon to changes in $CO_2$, and the carbon-climate sensitivity ($\gamma$), quantifying the sensitivity to subsequent climate changes.

Following Friedlingstein et al. (2003), the change in global land and ocean carbon storage is assumed to be linear with increases in $CO_2$ and also with global warming. Therefore, the future changes in land carbon storage ($\Delta C_L$) and ocean carbon storage ($\Delta C_O$) are linearly approximated as the sum of contributions from increased $CO_2$ concentrations ($\Delta CO_2$) and global warming ($\Delta T$), as shown by Equations 1 (land) and 2 (ocean):

$$\Delta C_L = \beta_L \Delta CO_2 + \gamma_L \Delta T \tag{1}$$

$$\Delta C_O = \beta_O \Delta CO_2 + \gamma_O \Delta T \tag{2}$$

where the sensitivity parameters for land and ocean are given by $\beta_L$, $\gamma_L$ and $\beta_O$, $\gamma_O$, respectively. Since CMIP5, the $C^4$MIP 1% $CO_2$ simulations have been used as the standard method for calculating these parameters. To define the $\beta$ parameters, the sensitivity of carbon storage to $CO_2$ is calculated at a specific $CO_2$ concentration (i.e., 2×$CO_2$ or 4×$CO_2$) using the BGC runs (isolating the direct $CO_2$ sensitivities). The $\gamma$ parameters are estimated using the sensitivity of carbon storage to subsequent global warming, calculated using the

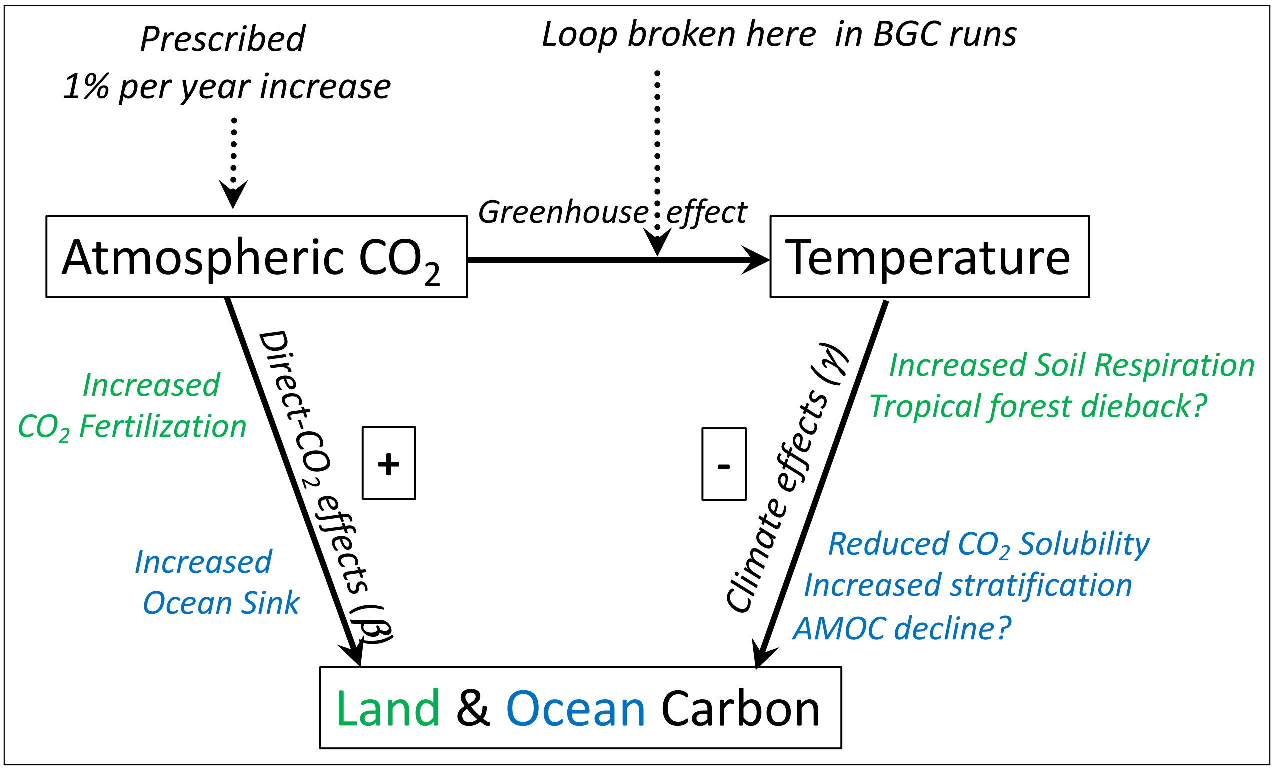


**Figure 1** Schematic diagram showing the key interactions quantified in C4MIP climate-carbon cycle runs. In the latest versions of C4MIP, $CO_2$ is not an internal model variable but is instead prescribed to increase by 1% per year. In the coupled runs, $CO_2$ affects land and ocean carbon storage both directly ('$\beta$-effects'), and indirectly, as a result of the climate change caused by the $CO_2$ increase ('$\gamma$-effects'). In the BGC runs, the climate change effects are disabled by breaking the link between $CO_2$ and climate. In this study, climate effects are defined as the difference between the BGC and coupled runs.

| EARTH SYSTEM MODEL | 2×$CO_2$ | | | | 4×$CO_2$ | | | |
|---|---|---|---|---|---|---|---|---|
| | $\beta_L$ | $\gamma_L$ | $\beta_O$ | $\gamma_O$ | $\beta_L$ | $\gamma_L$ | $\beta_O$ | $\gamma_O$ |
| ACCESS-ESM1.5 | 0.75 | –12.0 | 1.06 | –11.7 | 0.37 | –21.1 | 0.90 | –23.8 |
| BCC-CSM2-MR | 2.22 | –132.8 | 1.09 | –12.4 | 1.81 | –163.1 | 0.92 | –19.9 |
| CESM2 | 0.98 | –12.8 | 0.84 | –4.24 | 0.90 | –21.6 | 0.71 | –10.9 |
| CNRM-ESM2-1* | 1.36 | –48.4 | 0.62 | –4.0 | 1.36 | –83.7 | 0.57 | –9.5 |
| CanESM5 | 1.42 | –6.22 | 0.90 | –7.71 | 1.28 | 16.0 | 0.77 | –14.7 |
| GFDL-ESM4 | 1.08 | –50.7 | 0.97 | –8.97 | 0.93 | –80.1 | 0.84 | –21.7 |
| IPSL-CM6A-LR | 1.11 | –12.2 | 0.87 | –7.37 | 0.62 | –8.7 | 0.76 | –13.0 |
| MIROC-ES2L | 1.45 | –63.4 | 0.85 | –10.4 | 1.12 | –69.6 | 0.73 | –22.3 |
| MPI-ESM1.2-LR | 1.08 | –0.81 | 0.88 | –11.4 | 0.71 | –5.17 | 0.77 | –20.1 |
| NorESM2-LM | 0.94 | –15.6 | 0.88 | –9.34 | 0.85 | –21.0 | 0.78 | –19.6 |
| UKESM1-0-LL | 1.00 | –24.0 | 0.88 | –7.35 | 0.75 | –38.4 | 0.75 | –14.1 |
| Ensemble mean | 1.22 | –34.1 | 0.91 | –8.59 | 0.97 | –45.1 | 0.78 | –17.2 |
| Ensemble SD | 0.40 | 38.4 | 0.09 | 2.90 | 0.40 | 50.6 | 0.07 | 5.0 |

**Table 1** Parameters for the old $\beta$-$\gamma$ formulation: land and ocean carbon-concentration ($\beta_{L,O}$ PgC ppm$^{-1}$) and carbon-climate ($\gamma_{L,O}$, PgC °C$^{-1}$) sensitivity parameters, shown for 2×$CO_2$ and 4×$CO_2$ in CMIP6 ESMs. As presented in Arora et al. (2020), but with $\gamma$ values shown to just one decimal place. *The parameters for CNRM-ESM2-1 were recalibrated for this study.

residual climate changes in the fully coupled simulations relative to the BGC runs (RES = COU – BGC). The $\beta$ and $\gamma$ parameters for the CMIP6 ESMs are presented in Table 1, taken from Arora et al. (2020). This method of separating direct-$CO_2$ ($\beta$) effects and climate ($\gamma$) effects is demonstrated schematically in Figure 1.

The quantification of land and ocean carbon cycle sensitivities in this way has been useful to identify the zeroth-order reasons for differences between ESM projections and provides a useful comparison between CMIP model generations (Canadell et al., 2021). As ESMs increase in complexity, the $\beta$–$\gamma$ formulation allows for the simple quantification of carbon cycle sensitivities for a given increase in atmospheric $CO_2$. The framework can be applied to concentration-driven and emission-driven simulations and accounts for the differences due to climate sensitivities (Gregory et al., 2009; Varney et al., 2024). More recently, the $\beta$-$\gamma$ formulation has also been linked to policy-relevant metrics such as the relationship of global warming to both cumulative carbon emissions (TCRE; Jones and Friedlingstein (2020)) and the 'Zero Emissions Commitment' (ZEC; Jones et al. (2019)).

Despite this, a key limitation of the $\beta$–$\gamma$ formulation is the assumption of $\Delta C_L$ and $\Delta C_O$ being linear with both increasing $CO_2$ and temperature. For this assumption to be valid, the $\beta$ and $\gamma$ parameter values should be consistent regardless of the $CO_2$ levels over which they are calculated (i.e., 2×$CO_2$ or 4×$CO_2$). However, these parameters vary if calculated using either 2×$CO_2$ or 4×$CO_2$ (Arora et al., 2020; Varney et al., 2024). In general, $\beta$ values are smaller and $\gamma$ values are more negative at 4×$CO_2$. This is indicative of sink saturation at high $CO_2$ (see Figure S.1), which cannot be captured by the linear $\beta$–$\gamma$ formulation.

## 3 A MORE ROBUST DIAGNOSIS OF CARBON CYCLE FEEDBACKS

The assumption that increases in land and ocean carbon storage are proportional to changes in atmospheric $CO_2$ concentration is inconsistent with our understanding and modelling of the processes that lead to sink saturation at high $CO_2$, as explained in Section 1. Also, the standard $\beta$–$\gamma$ formulation does not represent the timescales involved in carbon uptake by the land and ocean, instead assuming an instantaneous adjustment of carbon stores. It therefore predicts the same increase in land and ocean carbon storage as a function of the $CO_2$ concentration and global warming, regardless of the scenario used to get to that state. This is at odds with the outputs of complex ESMs, which show a dependence of carbon storage on the rate of increase of $CO_2$ (Canadell et al., 2021; Melnikova et al., 2021; Varney et al., 2023). In this paper, we seek to improve the standard $\beta$–$\gamma$, by representing sink saturation, and also the characteristic timescales of land and ocean carbon uptake.

We aim to improve the standard formulation by relaxing each of these assumptions in turn, in a way that minimises the additional complexity introduced. We design our new approach so that it requires no additional model runs in addition to those required by the standard approach. That is, we continue to deduce the carbon-concentration sensitivity from the BGC runs, and the carbon-climate sensitivity from the difference between the fully coupled and the biogeochemically coupled runs.

### 3.1 THE NEW $\beta$–$\gamma$–$\kappa$–$\tau$ DIAGNOSIS OF CARBON CYCLE SENSITIVITIES

In order to reduce the scenario sensitivity of the standard $\beta$–$\gamma$ formulation, we introduce timescales, $\tau_i$, to account for the response times of the land and ocean carbon stores:

$$\frac{dC_i}{dt} = \frac{\Delta C_i^{eq} - \Delta C_i}{\tau_i} \tag{3}$$

where $i$ represents land or ocean, and $\Delta$ values are relative to the initial state. Equation 3 represents the rate of land and ocean carbon uptake (left-hand side), as a result of the related carbon stores being out of equilibrium with the atmospheric $CO_2$ concentration and the climate (right-hand side). The time-varying equilibrium change in the carbon stores is represented by $\Delta C_i^{eq}$, which is time-varying by virtue of time-varying changes in $CO_2$ and climate. Hereafter, we call $\Delta C_i^{eq}$ the 'quasi-equilibrium' change in the carbon stores. The uptake rate depends on how far the carbon stores, $\Delta C_i$, are from this quasi-equilibrium state, $\Delta C_i^{eq}$, and on the characteristic timescale of the system response, $\tau_i$. For small timescales, $\tau_i$, Equation 3 implies that $\Delta C_i \approx \Delta C_i^{eq}$, such that the carbon stores follow the time-varying quasi-equilibrium, as implied by the original $\beta$–$\gamma$ formulation (Friedlingstein et al., 2001).

In general, there are multiple timescales for carbon uptake by both land and ocean (Canadell et al., 2021). However, in the interests of limiting the number of additional parameters required for our new approach, we seek single values of $\tau_i$ for both land and ocean that allow us to significantly improve the fit to the standard $C^4$MIP runs (Arora et al., 2020). For land, the natural choice for $\tau_L$ is the effective turnover time for land carbon, given by the ratio of the mean land carbon to the mean net primary productivity (NPP):

$$\tau_L = \frac{\langle C_L \rangle}{\langle \mathrm{NPP} \rangle} \tag{4}$$

Best estimates of $\tau_L$ are therefore likely to come from mean values of global NPP and global land carbon over a pre-industrial control run. However, we find that these values are very well reproduced using the data from the first year of the $C^4$MIP coupled run (see Figure S.2). Guided by the principle that our new approach should not require significantly additional analysis, we therefore choose to use the first year of the $C^4$MIP coupled run to estimate $\tau_L$.

The issue of multiple timescales is even more relevant for the ocean carbon cycle (Sarmiento and Toggweiler, 1984; Strassmann and Joos, 2018). However, the increase in ocean carbon storage in response to an abrupt 4×$CO_2$ change is similar across the $C^4$MIP models, and is broadly consistent with 15%, 60% and 25% of the total ocean carbon uptake occurring with characteristic timescales of 10, 100, and 1000 years, respectively (see Figure S.3(a)). Since we aim to fit the $C^4$MIP models on the decadal to century timescale, we choose $\tau_o = 100$ years, which approximately reproduces the

| MODEL | LAND | | | | OCEAN | | | |
|---|---|---|---|---|---|---|---|---|
| | $\beta_L$ | $\gamma_L$ | $\kappa_L$ | $\tau_L$ | $\beta_O$ | $\gamma_O$ | $\kappa_O$ | $\tau_O$ |
| ACCESS-ESM1.5 | 6.8 | –26 | 46 | 36.5 | 6.0 | –50 | 307 | 100 |
| BCC-CSM2-MR | 5.3 | –234 | 532 | 44.2 | 6.0 | –45 | 323 | 100 |
| CESM2 | 3.0 | –33 | 659 | 53.0 | 5.0 | –24 | 291 | 100 |
| CNRM-ESM2-1 | 4.1 | –153 | 904 | 55.5 | 3.3 | –25 | 418 | 100 |
| CanESM5 | 3.4 | 17 | 828 | 33.5 | 5.4 | –36 | 297 | 100 |
| GFDL-ESM4 | 2.0 | –82 | 1022 | 18.7 | 6.1 | –46 | 290 | 100 |
| IPSL-CM6A-LR | 3.4 | –12 | 218 | 25.2 | 5.6 | –30 | 310 | 100 |
| MIROC-ES2L | 3.9 | –94 | 476 | 35.3 | 5.2 | –51 | 317 | 100 |
| MPI-ESM1-2-LR | 2.6 | –7 | 383 | 22.7 | 5.0 | –45 | 351 | 100 |
| NorESM2-LM | 4.7 | –50 | 397 | 86.2 | 5.3 | –51 | 337 | 100 |
| UKESM1-0-LL | 3.1 | –55 | 366 | 39.6 | 5.4 | –33 | 285 | 100 |
| Ensemble mean | 3.8 | –66 | 530 | 40.9 | 5.3 | –40 | 321 | 100.0 |
| Ensemble SD | 1.4 | 73 | 298 | 19.0 | 0.8 | 10 | 38 | 0.0 |

**Table 2** Best-fit values for the new $\beta$–$\gamma$–$\kappa$–$\tau$ formulation: initial carbon-concentration sensitivity, $\beta$ (PgC ppmv$^{-1}$), carbon-climate sensitivity, $\gamma$ (PgC K$^{-1}$), and half saturation constant, $\kappa$ (ppmv), for land and ocean carbon uptake in each of the C$^4$MIP models. Also shown are the characteristic timescales, $\tau$ (years), for land and ocean, although these are not fitting parameters. We fix $\tau_O = 100$ years for all the models, and diagnose $\tau_L$ for each model from the initial land carbon and NPP—see Section 3.1.

declining ocean carbon sink for years 20 to 120 in the abrupt 4×$CO_2$ runs (see Figure S.3(b)).

Given $\tau_i$, we can use $\Delta C_i$ to estimate the time-evolution of the underlying quasi-equilibrium states:

$$\Delta C_i^{eq} = \Delta C_i + \tau_i \frac{dC_i}{dt} \tag{5}$$

The next stage of our simple extension of the $\beta$–$\gamma$ formulation is to introduce a saturating response of these quasi-equilibrium carbon stores to $CO_2$:

$$\Delta C_i^{eq} = \frac{\beta_i \kappa_i \Delta CO_2}{\Delta CO_2 + \kappa_i} + \gamma_i \Delta T \tag{6}$$

Here $\kappa_i$ is a half-saturation constant representing the $\Delta CO_2$ value that yields half of the maximum 'saturating' response to $CO_2$. If the $CO_2$ level is much lower than $\kappa_i$, Equation 6 reduces to the form of the original $\beta$-$\gamma$ formulation (i.e., Equations 1 and 2) Conversely, if $\Delta CO_2$ is much larger than $\kappa_i$, then $\Delta C^{eq}$ becomes insensitive to changes in $CO_2$. This functional form is reminiscent of Michaelis–Menten kinetics, ubiquitous in biological applications, and is also one of the simplest ways to capture sink saturation.

Once $\tau_i$ has been assumed, it is possible to estimate the time evolution of quasi-equilibrium carbon storage values using Equation 5, and we do this using standard C$^4$MIP runs: coupled runs ('COU'; climate and $CO_2$ affecting carbon stores); and the $CO_2$-only runs ('BGC'; only $CO_2$ affecting carbon stores). As for the standard $\beta$–$\gamma$ approach, we assume that $\Delta T$ effects are negligible in the BGC run, so we can fit $\beta_i$ and $\kappa_i$ to the estimated quasi-equilibrium values for the BGC runs, without needing to know $\gamma_i$. The residual of the quasi-equilibrium from the COU runs, and this fit to the quasi-equilibrium value from the BGC runs, is then fitted to $\gamma_i \Delta T$. Fits were carried out in *python* using the *curve fit* routine. Best-fit parameters are shown in Table 2, with uncertainties in the fitted sensitivity parameters given in Table S.1.

## 3.2 RESULTS

Figure 2 shows global changes from the coupled runs (COU) of the CMIP6 generation of C$^4$MIP (Arora et al., 2020). As for the previous CMIP5 generation of C$^4$MIP (Arora et al., 2013), all modelling groups were required to prescribe a 1% per year increase in $CO_2$ from a preindustrial $CO_2$ concentration of about 284 ppmv to at least four times that value (panel (a)). As the models have rather different climate sensitivities to $CO_2$ (Nijsse et al., 2020), this common $CO_2$ scenario still leads to a wide range of global warming projections, ranging from about 4K (NorESM2-LM, MIROC-ES2L, GFDL-ESM4) to about 7K (CanESM5, UKESM1-0-LL, IPSL-CM6-LR) at 4×$CO_2$ (panel (b)). The $CO_2$ increase and global warming lead to significant changes in the land and ocean carbon cycles in the models. On the land, global NPP increases in all models, primarily due to $CO_2$-fertilisation of photosynthesis. However, the extent of the NPP increase varies hugely across the models from less than 10% (ACCESS-ESM1-5) to almost 150% (CanESM5), most likely due to differing levels of nutrient limitations. As a result, the change in global land carbon also varies hugely across the models, from an increase of about 200 PgC (ACCESS-ESM1-5) to an increase in excess of 1300 PgC (CanESM5), as shown in panel (d). The model projections

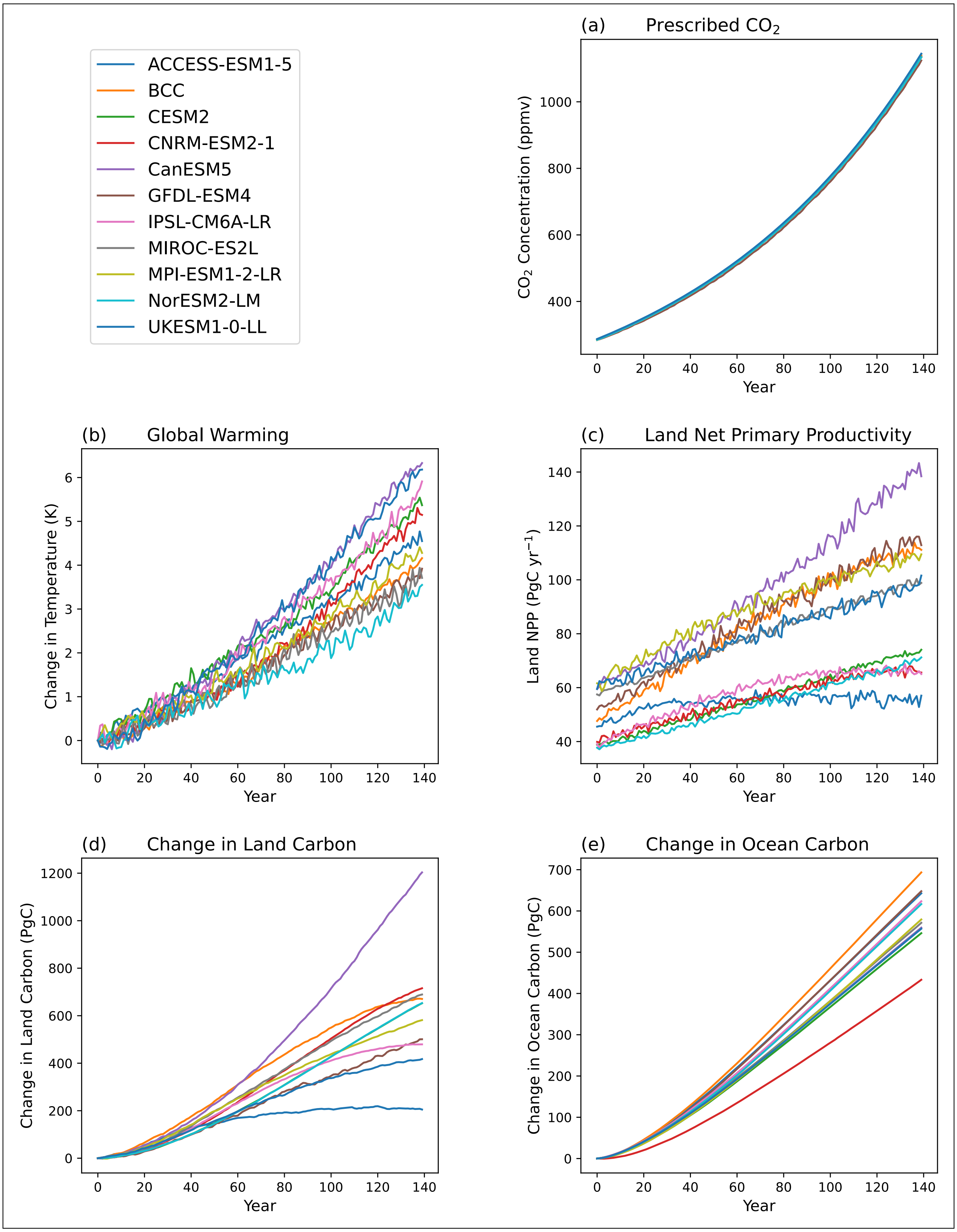


**Figure 2** Global variables from the C[4]MIP coupled runs: **(a)** prescribed 1% per year increase in atmospheric $CO_2$ concentration; **(b)** increase in global mean temperature; **(c)** global mean land net primary productivity; **(d)** change in land carbon storage; and **(e)** change in ocean carbon storage.

for changes in ocean carbon storage are more clustered, but still range from a little more than 400 PgC (CNRM-ESM2-1) to over 750 PgC (BCC). In general, most models show evidence of saturation of $CO_2$ effects on NPP and the change in land carbon (the only exception being CanESM5). Sink saturation effects in the ocean carbon uptake are not immediately evident in panel (e). However, panel (e) does reveal a lagged ('cold-start') in ocean uptake, for all models.

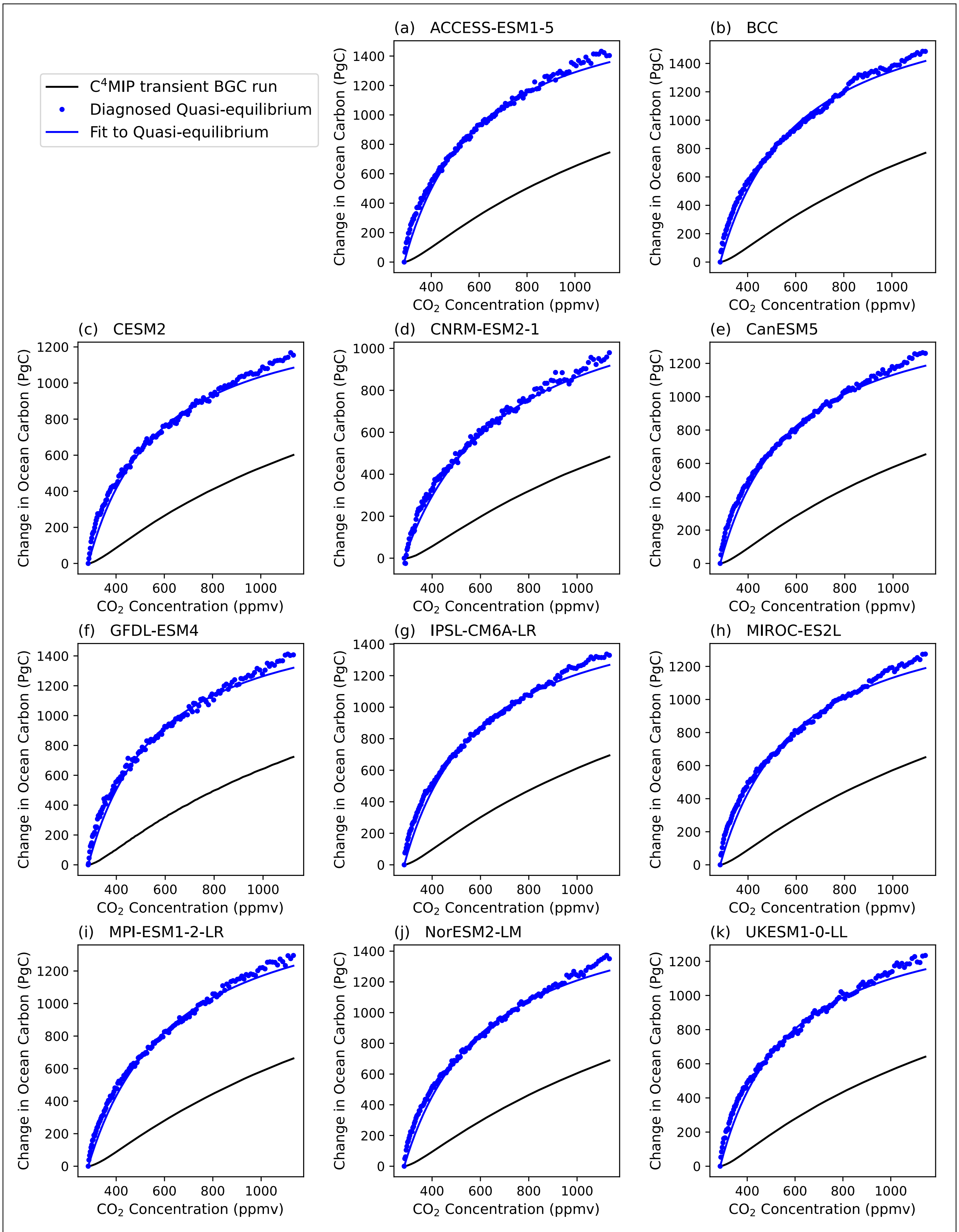


**Figure 3** Fitting procedure for the $CO_2$ response of the change in global ocean carbon storage, with a panel for each of the $C^4$MIP models. Each panel shows the change in global mean ocean carbon from the $C^4$MIP BGC run (black line); the quasi-equilibrium state inferred assuming a characteristic lifetime of 100 years in each model (blue dots); and our two-parameter fit to this quasi-equilibrium response (blue line).

This is indicative of a non-negligible characteristic timescale for ocean carbon uptake, which hides the sink saturation effects, as we show below.

In order to reveal the sink saturation, we estimate the quasi-equilibrium state from Equation 5. Figure 3 shows the original transient BGC $C^4$MIP runs (black lines), and this reconstructed quasi-equilibrium state (blue dots), with one panel for each of the $C^4$MIP models. Now, ocean sink saturation is clearly seen in the reconstructed quasi-equilibrium of every model. We can now compare these quasi-equilibrium responses to the saturating $CO_2$ response of Equation 6 using the estimated values of $\beta_o$ and $\kappa_o$. These reconstructions are shown by the blue lines in Figure 3 (and we do likewise for land carbon, see Supplementary Material, Figure S.4).

Figure 4 shows a similar process for the climate response of land carbon. Here the climate response (shown by black dots) is diagnosed as the difference between the coupled runs (COU) and the BGC runs. We plot this residual against the temperature anomaly from the coupled run. In general, $CO_2$-only responses are smoother (see Figure 3 for the ocean and Figure S.4 for the land), while climate-only responses show more scatter, especially for the land (see Figure 4 for the land and Figure S.5 for the ocean). However, all models show continuous reductions in the rate of land carbon uptake due to global warming, apart from CanESM5 for which the diagnosed climate change effect is negative to start with and then switches to become positive beyond a global warming of approximately 4°C. As for ocean carbon uptake, models show evidence of lags in their responses, which introduces a curvature in the line linking the black dots (see Supplementary Material, Figure S.5). Again, we can estimate the quasi-equilibrium response using Equation 5 and the characteristic timescales diagnosed using Equation 4. The red dots in Figure 4 show this reconstructed quasi-equilibrium response for each model, which is always more linear in global warming than the transient response (black dots). The fitted straight line for the quasi-equilibrium response, with gradient $\gamma_L$, is also shown. We do likewise for $\gamma_O$ for each model (Figure S.5).

Table 2 shows the best-fit parameters for each model using our new $\beta$–$\gamma$–$\kappa$–$\tau$ method, and Figure S.6 compares the new $\beta$ and $\gamma$ values with the old ones. It should be noted here that the $\beta$ parameters in the old and new approach are not directly comparable. In the new approach $\beta$ defines the initial sensitivity of the carbon store to $CO_2$, from the pre-industrial $CO_2$ concentration. In the old approach, $\beta$ relates to the mean impact of $CO_2$ on the carbon stores from pre-industrial to 2×$CO_2$ or 4×$CO_2$. As a result of sink saturation, which is neglected in the standard $\beta$–$\gamma$ approach, the new $\beta$ values are much larger. For the new approach, as with the old, we see more variation in the best-fit parameters for land carbon than for ocean carbon. Indeed, there is a good deal of model agreement on the ocean carbon responses to both $CO_2$ and climate. For both land and ocean, it is notable that the new fit implies more negative land and ocean responses to global warming (ensemble mean $\gamma_L$ moves from –45±51 PgC/K to –66±73 PgC/K; ensemble mean $\gamma_O$ moves from –17±5 PgC/K to –40±10 PgC/K). This is primarily due to fitting to diagnosed quasi-equilibrium states rather than the dynamical evolution of the carbon stores (see Figures 4 and S.5).

Figure 5 shows the fit of the new $\beta$-$\gamma$-$\kappa$-$\tau$ approach (thick dashed lines) to the changes in land and ocean storage in the coupled C$^4$MIP runs (thick continuous lines). For comparison, we also show the old $\beta$-$\gamma$ fits (thin continuous lines). It is clear that the new approach picks up the sink saturation effects that are evident in the C$^4$MIP outputs but which cannot be captured by the linear $\beta$-$\gamma$ approach. This is further evidenced by Figure 6, which shows root mean square errors (RMSEs) for the old and new approaches relative to the C$^4$MIP outputs. With the single exception of the change in land carbon in CanESM5 (which is unusually linear when plotted against $CO_2$), RMSEs are reduced significantly for all models and for both land and ocean, in the new approach. The improvement in the quality of the fit for land carbon uptake is especially impressive, with mean RMSE reduced by the new approach from about 70 PgC in the old approach, to about 17 PgC in the new.

## 4 DISCUSSION

Our extension to the old $\beta$–$\gamma$ model rests on four key assumptions. First, we assume that the quasi-equilibrium response can be reconstructed from the transient response using a single timescale. This assumption is more justifiable for land carbon than for ocean carbon, as ocean uptake is known to respond on multiple timescales (Canadell et al., 2021; Sarmiento and Toggweiler, 1984; Strassmann and Joos, 2018). To demonstrate this, we examine how well our new fit predicts the land and ocean carbon uptake 120 years after an abrupt quadrupling of $CO_2$ (i.e., by examining the abrupt 4×$CO_2$ runs with the C$^4$MIP models). Figure S.7 shows that our $\beta$–$\gamma$–$\kappa$–$\tau$ fit to the 1% year runs does surprisingly well in predicting the land uptake in the 4×$CO_2$ runs (see Figure S.7a). However, the assumption of a single timescale of the ocean response tends to overestimate carbon uptake 120 years after the abrupt $CO_2$ increase (see Figure S.7b).

Second, we assume that the single timescale for land is approximated by the ratio of the equilibrium land carbon to the equilibrium NPP. The quality of the fits to the 1% per year runs (see Figure S.4), and the ability to approximately reproduce the abrupt 4×$CO_2$ response (see Figure S.7a), suggest that this is a good assumption for the land. Thirdly, we assume that a single ocean timescale of 100 years is sufficient to identify the decadal-to-century timescale quasi-equilibrium response of the ocean. This is arguably the biggest weakness of our $\beta$–$\gamma$–$\kappa$–$\tau$ approach. It is an assumption that we have made in our attempt to develop a transparently simple extension to the existing $\beta$–$\gamma$ formulation, but one that warrants further analysis in the future.

Finally, we assume that the quasi-equilibrium response to $CO_2$ approximates a (Michaelis–Menton-like) hyperbolic response. The quality of the fit of the saturating hyperbolic to the diagnosed quasi-equilibrium from the $CO_2$-only (BGC) runs suggests that this is a good assumption at least up to 900 ppmv for the ocean (see Figure 3), and for most land models up to 4×$CO_2$ (see Figure S.4). The exceptions are ACCESS-ESM1.5 and IPSL-CM6A-LR, which show a loss of the quasi-equilibrium land carbon sink at high $CO_2$ even in

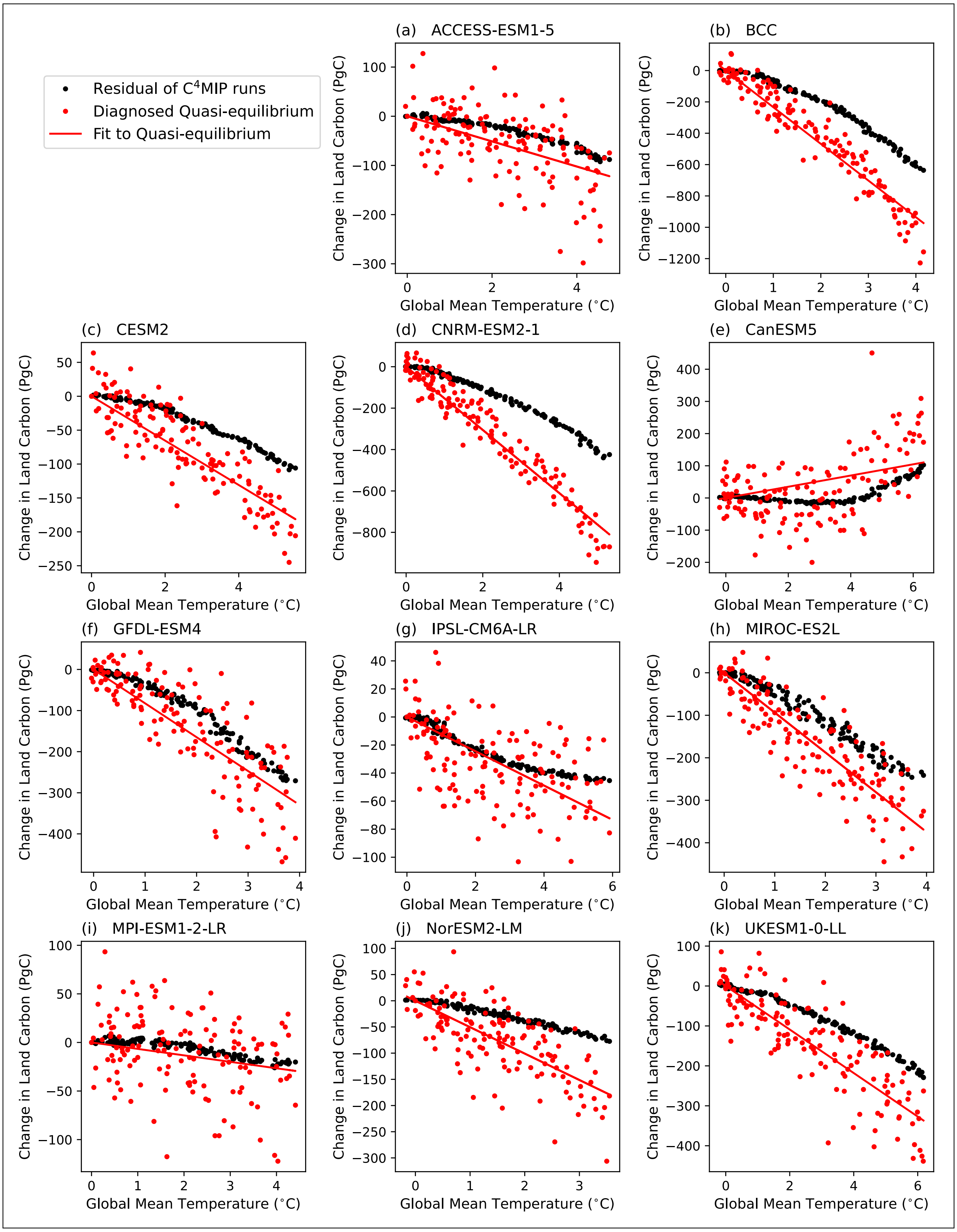


**Figure 4** Fitting procedure for the climate response of global land carbon storage, with a panel for each of the C4MIP models. Each panel shows the change in global mean land carbon against global warming, calculated as the difference between the C4MIP BGC and coupled runs (black line); the quasi-equilibrium state inferred assuming a characteristic lifetime for land carbon in each model (red dots); and a linear fit to this quasi-equilibrium response (red line).

the absence of climate change effects. This may be indicative of these models having characteristic timescales that are not well approximated by the ratio of the equilibrium land carbon to equilibrium NPP.

Despite these simplifications within our new $\beta$–$\gamma$–$\kappa$–$\tau$ approach, it reproduces the C4MIP 1% per year runs much better than the existing $\beta$–$\gamma$ approach without requiring any new runs to be analysed.

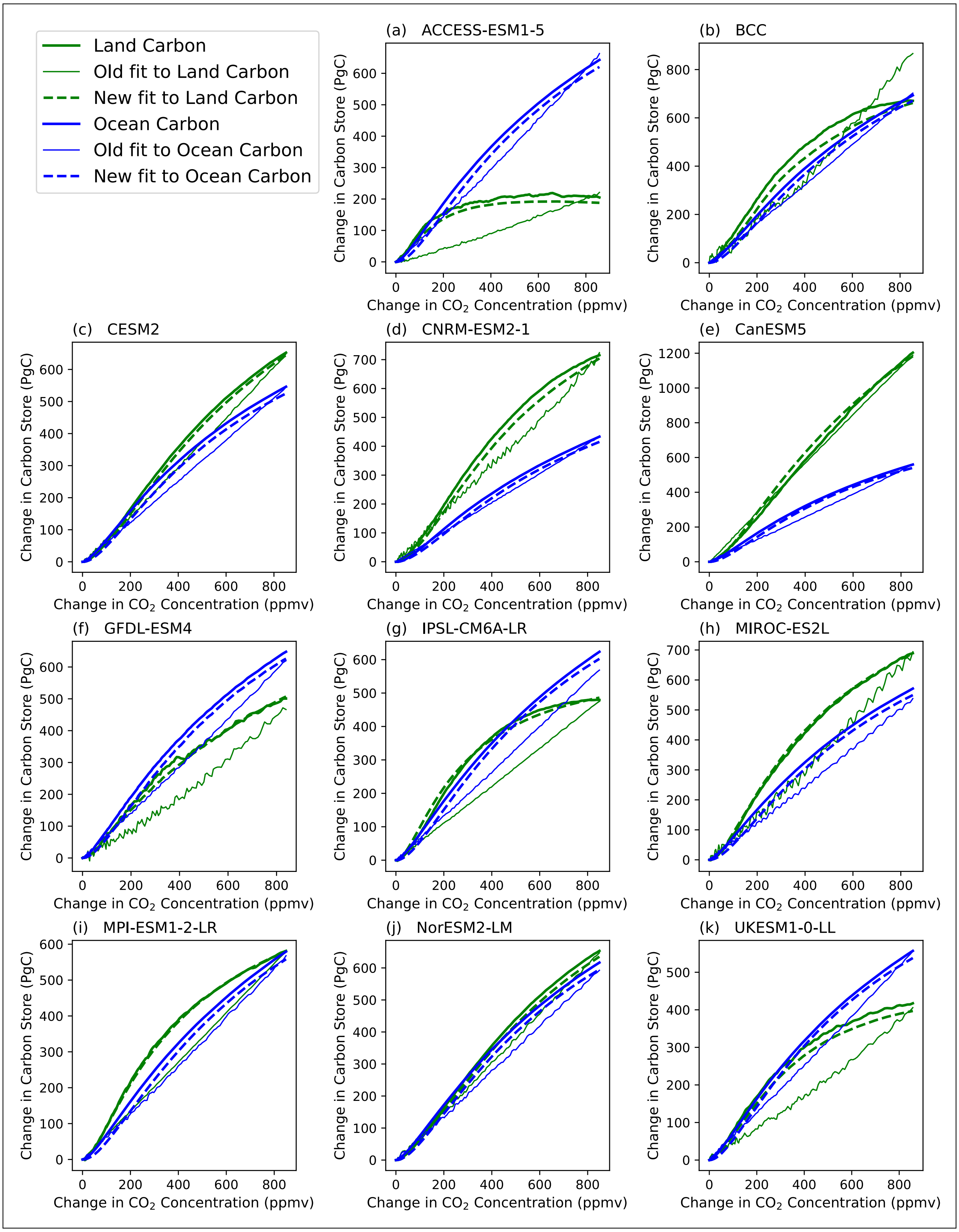


**Figure 5** Comparison of fits to the change in land carbon storage (green lines) and ocean carbon storage (blue lines) for the coupled runs (thick continuous lines). Fits are shown for both the old $\beta$–$\gamma$ model (thin continuous lines) and our new $\beta_0$–$\gamma$–$\kappa$–$\tau$ model (thick dashed lines).

## 5 CONCLUSIONS

The carbon cycle and the climate system interact on timescales from seasonal to multi-millennial. Over the last 25 years, GCMs of the climate have started to include models of the land and ocean carbon cycle as interactive components. These models indicate that carbon cycle feedbacks on future climate change could be very important, but differences between models remain, especially in the response of the land carbon cycle to increases in $CO_2$ and changes in

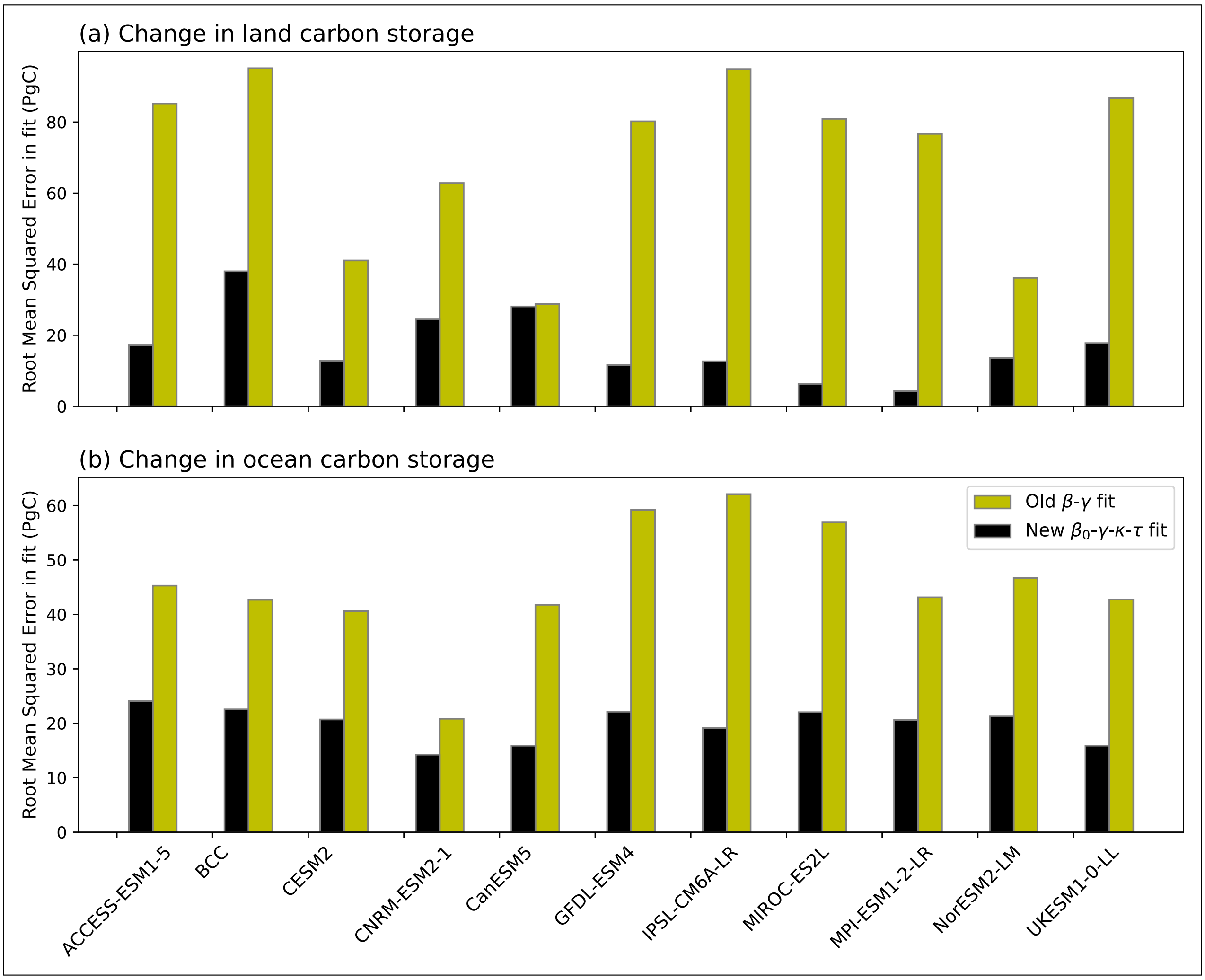


**Figure 6** Root mean square errors in the fits of the old $\beta$–$\gamma$ model (yellow bars), and the new $\beta_0$–$\gamma$–$\kappa$–$\tau$ model (black bars), for each of the $C^4$MIP models: **(a)** change in land carbon; **(b)** change in ocean carbon.

climate. Reducing the remaining uncertainties will require a combination of better diagnosis, improvements in model process representation, and better model calibration. Until now, the diagnosis of the sources of differences between ESMs has relied on an assumption that changes in land and ocean carbon storage respond approximately linearly to changes in atmospheric $CO_2$ and global warming (the '$\beta$–$\gamma$' framework). In this paper, we have shown that the results from ESMs instead show strong evidence of sink saturation at high-$CO_2$, which cannot be captured by the standard $\beta$–$\gamma$ approach. We have therefore developed a simple extension to the existing approach to capture sink saturation and the characteristic timescales of carbon uptake by the land and ocean. The resulting $\beta$–$\gamma$–$\kappa$–$\tau$ provides a much improved fit to the outputs from complex coupled climate-carbon cycle GCMs. We hope that our new approach will be helpful in analysing the varying carbon cycle responses across different models, and between model generations. The representation of sink saturation effects within our approach should make it easier to identify the impact of new process representations such as nutrient limitations. In addition, it is vital to keep sink saturation in mind when considering future carbon sinks, and our new $\beta$–$\gamma$–$\kappa$–$\tau$ approach allows these effects to be much more clearly diagnosed.

## CODE AVAILABILITY

Code accompanying this paper can be found on GitHub at https://github.com/josephjclarke/ClimateCarbonCycleFeedbacks.

## DATA AVAILABILITY

The CMIP6 Earth system model output data is available online: https://esgf-node.ipsl.upmc.fr/projects/cmip6-ipsl/ and the $C^4$MIP data used in Arora et al. (2020) is available at: https://c4mip.net/results.

## ADDITIONAL FILE

The additional file for this article can be found as follows:

- **Supplementary Material.** Figures S1 to S7 and Table S1. DOI: https://doi.org/10.16993/tellus.4128.s1

## FUNDING INFORMATION

PMC was supported by the European Union's Horizon Europe research and innovation programme under grant agreement numbers 101137601 (ClimTip) and 101184989 (NextGenCarbon). JJC acknowledges support from the ESA PREDICT project (Contract No. 4000146344/24/I-LR). SRGJ acknowledges support from the NERC funded QUINTUS project (NE/S015833/1). RMV was supported by the Schmidt Sciences CALIPSO project.

## COMPETING INTERESTS

The authors have no competing interests to declare.

## AUTHOR CONTRIBUTIONS

PMC conceived of the new $\beta$–$\gamma$–$\kappa$–$\tau$ approach and designed the study. JJC processed the $C^4$MIP models data and drafted Section 3. SJ drafted Section 1 and RMV drafted Section 2 of the paper. All authors contributed to the study and to the submitted paper.

## AUTHOR AFFILIATIONS

**Peter M. Cox** orcid.org/0000-0002-0679-2219
Faculty of Environment, Science and Economy, University of Exeter, Exeter, UK; Global Systems Institute, University of Exeter, Exeter, UK

**Joseph J. Clarke** orcid.org/0000-0002-6250-1543
Faculty of Environment, Science and Economy, University of Exeter, Exeter, UK; Global Systems Institute, University of Exeter, Exeter, UK

**Simon R. G. Jones** orcid.org/0000-0002-2653-2318
Faculty of Environment, Science and Economy, University of Exeter, Exeter, UK; Global Systems Institute, University of Exeter, Exeter, UK

**Rebecca M. Varney** orcid.org/0000-0002-0637-0841
Department of Physical Geography, Stockholm University, Stockholm, Sweden; Bolin Centre for Climate Research, Stockholm University, Stockholm, Sweden

## REFERENCES

**Arora, V. K., Boer, G. J., Friedlingstein, P., Eby, M., Jones, C. D., Christian, J. R., Bonan, G., Bopp, L., Brovkin, V., Cadule, P.,** et al. (2013). Carbon–concentration and carbon–climate feedbacks in CMIP5 Earth system models. *Journal of Climate*, *26*(15), 5289–5314. https://doi.org/10.1175/JCLI-D-12-00494.1

**Arora, V. K., Katavouta, A., Williams, R. G., Jones, C. D., Brovkin, V., Friedlingstein, P., Schwinger, J., Bopp, L., Boucher, O., Cadule, P.,** et al. (2020). Carbon–concentration and carbon–climate feedbacks in CMIP6 models and their comparison to CMIP5 models. *Biogeosciences*, *17*(16), 4173–4222. https://doi.org/10.5194/bg-17-4173-2020

**Ball, J. T., Woodrow, I. E.,** & **Berry, J. A.** (1987). A model predicting stomatal conductance and its contribution to the control of photosynthesis under different environmental conditions. In *Progress in photosynthesis research: volume 4 proceedings of the VIIth international congress on photosynthesis providence, Rhode Island, USA, august 10–15, 1986*, (pp. 221–224). Springer. https://doi.org/10.1007/978-94-017-0519-6_48

**Betts, R. A., Cox, P. M., Lee, S. E.,** & **Woodward, F. I.** (1997). Contrasting physiological and structural vegetation feedbacks in climate change simulations. *Nature*, *387*(6635), 796–799. https://doi.org/10.1038/42924

**Bolin, B.** (1977). Changes of Land Biota and Their Importance for the Carbon Cycle: The increase of atmospheric carbon dioxide may partly be due to the expansion of forestry and agriculture. *Science*, *196*(4290), 613–615. https://doi.org/10.1126/science.196.4290.613

**Bolin, B., Björkström, A.,** & **Moore, B.** (1989). Uptake by the Atlantic Ocean of excess atmospheric carbon dioxide and radiocarbon. *Understanding Climate Change*, *52*, 57–78. https://doi.org/10.1029/GM052p0057

**Canadell, J., Monteiro, P., Costa, M., Cotrim da Cunha, L., Cox, P., Eliseev, A., Henson, S., Ishii, M., Jaccard, S., Koven, C., Lohila, A., Patra, P., Piao, S., Rogelj, J., Syampungani, S., Zaehle, S.,** & **Zickfeld, K.** (2021). *Global carbon and other biogeochemical cycles and feedbacks*. Cambridge University Press.

**Cox, P., Betts, R., Bunton, C., Essery, R., Rowntree, P.,** & **Smith, J.** (1999). The impact of new land surface physics on the GCM simulation of climate and climate sensitivity. *Climate Dynamics*, *15*(3), 183–203. https://doi.org/10.1007/s003820050276

**Cox, P. M.** (2001). Description of the "TRIFFID" dynamic global vegetation model. Hadley Centre Technical Note 24, Met Office, UK. https://library.metoffice.gov.uk/Portal/Default/en-GB/RecordView/Index/252319

**Cox, P. M., Betts, R., Collins, M., Harris, P. P., Huntingford, C.,** & **Jones, C.** (2004). Amazonian forest dieback under climate-carbon cycle projections for the 21st century. *Theoretical and applied climatology*, *78*(1), 137–156. https://doi.org/10.1007/s00704-004-0049-4

**Cox, P. M., Betts, R. A., Jones, C. D., Spall, S. A.,** & **Totterdell, I. J.** (2000). Acceleration of global warming due to carbon-cycle feedbacks in a coupled climate model. *Nature*, *408*(6809), 184–187. https://doi.org/10.1038/35041539

**Cramer, W., Bondeau, A., Woodward, F. I., Prentice, I. C., Betts, R. A., Brovkin, V., Cox, P. M., Fisher, V., Foley, J. A., Friend, A. D.,** et al. (2001). Global response of terrestrial ecosystem structure and function to CO2 and climate change: Results from six dynamic global vegetation models. *Global change biology*, *7*(4), 357–373. https://doi.org/10.1046/j.1365-2486.2001.00383.x

**Egleston, E. S., Sabine, C. L.,** & **Morel, F. M. M.** (2010). Revelle revisited: Buffer factors that quantify the response of ocean chemistry to changes in DIC and alkalinity. *Global*

*Biogeochemical Cycles*, *24*(1). https://agupubs.onlinelibrary.wiley.com/doi/abs/10.1029/2008GB003407

**Friedlingstein, P., Bopp, L., Ciais, P., Dufresne, J.-L., Fairhead, L., LeTreut, H., Monfray, P.,** & **Orr, J.** (2001). Positive feedback between future climate change and the carbon cycle. *Geophysical Research Letters*, *28*(8), 1543–1546. https://doi.org/10.1029/2000GL012015

**Friedlingstein, P., Cox, P., Betts, R., Bopp, L., von Bloh, W., Brovkin, V., Cadule, P., Doney, S., Eby, M., Fung, I.,** et al. (2006). Climate–carbon cycle feedback analysis: results from the C4MIP model intercomparison. *Journal of climate*, *19*(14), 3337–3353. https://doi.org/10.1175/JCLI3800.1

**Friedlingstein, P., Dufresne, J.-L., Cox, P.,** & **Rayner, P.** (2003). How positive is the feedback between climate change and the carbon cycle? *Tellus B: Chemical and Physical Meteorology*, *55*(2), 692–700. https://doi.org/10.3402/tellusb.v55i2.16765

**Friedlingstein, P., Fung, I., Holland, E., John, J., Brasseur, G., Erickson, D.,** & **Schimel, D.** (1995). On the contribution of CO2 fertilization to the missing biospheric sink. *Global Biogeochemical Cycles*, *9*(4), 541–556. https://doi.org/10.1029/95GB02381

**Friedlingstein, P., Meinshausen, M., Arora, V. K., Jones, C. D., Anav, A., Liddicoat, S. K.,** & **Knutti, R.** (2014). Uncertainties in CMIP5 climate projections due to carbon cycle feedbacks. *Journal of Climate*, *27*(2), 511–526. https://doi.org/10.1175/JCLI-D-12-00579.1

**Friedlingstein, P., O'Sullivan, M., Jones, M. W., Andrew, R. M., Hauck, J., Landschützer, P., Le Quéré, C., Li, H., Luijkx, I. T., Olsen, A.,** et al. (2024). Global Carbon Budget 2024. *Earth System Science Data Discussions*, *2024*, 1–133. https://doi.org/10.5194/essd-2024-519

**Gregory, J. M., Jones, C., Cadule, P.,** & **Friedlingstein, P.** (2009). Quantifying carbon cycle feedbacks. *Journal of Climate*, *22*(19), 5232–5250. https://doi.org/10.1175/2009JCLI2949.1

**Haxeltine, A.,** & **Prentice, I. C.** (1996). BIOME3: An equilibrium terrestrial biosphere model based on ecophysiological constraints, resource availability, and competition among plant functional types. *Global biogeochemical cycles*, *10*(4), 693–709. https://doi.org/10.1029/96GB02344

**Jones, C. D., Arora, V., Friedlingstein, P., Bopp, L., Brovkin, V., Dunne, J., Graven, H., Hoffman, F., Ilyina, T., John, J. G.,** et al. (2016). C4MIP–The coupled climate–carbon cycle model intercomparison project: Experimental protocol for CMIP6. *Geoscientific Model Development*, *9*(8), 2853–2880. https://doi.org/10.5194/gmd-9-2853-2016

**Jones, C. D.,** & **Friedlingstein, P.** (2020). Quantifying process-level uncertainty contributions to TCRE and carbon budgets for meeting Paris Agreement climate targets. *Environmental Research Letters*, *15*(7), 074019. https://doi.org/10.1088/1748-9326/ab858a

**Jones, C. D., Frölicher, T. L., Koven, C., MacDougall, A. H., Matthews, H. D., Zickfeld, K., Rogelj, J., Tokarska, K. B., Gillett, N. P., Ilyina, T.,** et al. (2019). The Zero Emissions Commitment Model Intercomparison Project (ZECMIP) contribution to C4MIP: Quantifying committed climate changes following zero carbon emissions. *Geoscientific Model Development*, *12*(10), 4375–4385. https://doi.org/10.5194/gmd-12-4375-2019

**Keeling, C. D.** (1960). The concentration and isotopic abundances of carbon dioxide in the atmosphere. *Tellus*, *12*(2), 200–203. https://onlinelibrary.wiley.com/doi/abs/10.1111/j.2153-3490.1960.tb01300.x

**Le Quéré, C., Orr, J. C., Monfray, P., Aumont, O.,** & **Madec, G.** (2000). Interannual variability of the oceanic sink of CO2 from 1979 through 1997. *Global Biogeochemical Cycles*, *14*(4), 1247–1265. https://doi.org/10.1029/1999GB900049

**LeBauer, D. S.,** & **Treseder, K. K.** (2008). Nitrogen limitation of net primary productivity in terrestrial ecosystems is globally distributed. *Ecology*, *89*(2), 371–379. https://esajournals.onlinelibrary.wiley.com/doi/abs/10.1890/06-2057.1

**Melnikova, I., Boucher, O., Cadule, P., Ciais, P., Gasser, T., Quilcaille, Y., Shiogama, H., Tachiiri, K., Yokohata, T.,** & **Tanaka, K.** (2021). Carbon cycle response to temperature overshoot beyond 2C: An analysis of CMIP6 models. *Earth's Future*, *9*(5), e2020EF001967. https://doi.org/10.1029/2020EF001967

**Nijsse, F. J., Cox, P. M.,** & **Williamson, M. S.** (2020). Emergent constraints on transient climate response (TCR) and equilibrium climate sensitivity (ECS) from historical warming in CMIP5 and CMIP6 models. *Earth System Dynamics*, *11*(3), 737–750. https://doi.org/10.5194/esd-11-737-2020

**Palmer, J.,** & **Totterdell, I.** (2001). Production and export in a global ocean ecosystem model. *Deep Sea Research Part I: Oceanographic Research Papers*, *48*(5), 1169–1198. https://doi.org/10.1016/S0967-0637(00)00080-7

**Petit, J.-R., Jouzel, J., Raynaud, D., Barkov, N. I., Barnola, J.-M., Basile, I., Bender, M., Chappellaz, J., Davis, M., Delaygue, G.,** et al. (1999). Climate and atmospheric history of the past 420,000 years from the Vostok ice core, Antarctica. *Nature*, *399*(6735), 429–436. https://doi.org/10.1038/20859

**Pitman, A.** (2003). The evolution of, and revolution in, land surface schemes designed for climate models. *International Journal of Climatology: A Journal of the Royal Meteorological Society*, *23*(5), 479–510. https://doi.org/10.1002/joc.893

**Prentice, I. C., Cramer, W., Harrison, S. P., Leemans, R., Monserud, R. A.,** & **Solomon, A. M.** (1992). Special paper: A global biome model based on plant physiology and dominance, soil properties and climate. *Journal of Biogeography*, *19*(2), 117–134. https://doi.org/10.2307/2845499

**Randall, D. A., Bitz, C. M., Danabasoglu, G., Denning, A. S., Gent, P. R., Gettelman, A., Griffies, S. M., Lynch, P., Morrison, H., Pincus, R.,** et al. (2019). 100 years of earth system model development. *Meteorological Monographs*, *59*, 12–1. https://doi.org/10.1175/AMSMONOGRAPHS-D-18-0018.1

**Revelle, R.,** & **Suess, H. E.** (1957). Carbon dioxide exchange between atmosphere and ocean and the question of an increase of atmospheric CO2 during the past decades. *Tellus*, *9*(1), 18–27. https://onlinelibrary.wiley.com/doi/abs/10.1111/j.2153-3490.1957.tb01849.x

**Sarmiento, J. L.**, & **Toggweiler, J.** (1984). A new model for the role of the oceans in determining atmospheric $pCO_2$. *Nature*, *308*(5960), 621–624. https://doi.org/10.1038/308621a0

**Sellers, P., Randall, D., Collatz, G., Berry, J., Field, C., Dazlich, D., Zhang, C., Collelo, G.,** & **Bounoua, L.** (1996a). A revised land surface parameterization (SiB2) for atmospheric GCMs. Part I: Model formulation. *Journal of climate*, *9*(4), 676–705. https://doi.org/10.1175/1520-0442(1996)009<0676:ARLSPF>2.0.CO;2

**Sellers, P. J., Dickinson, R., Randall, D., Betts, A. K., Hall, F. G., Berry, J. A., Collatz, G., Denning, A., Mooney, H. A., Nobre, C. A.,** et al. (1997). Modeling the exchanges of energy, water, and carbon between continents and the atmosphere. *Science*, *275*(5299), 502–509. https://doi.org/10.1126/science.275.5299.502

**Sellers, P. J., Tucker, C. J., Collatz, G. J., Los, S. O., Justice, C. O., Dazlich, D. A.,** & **Randall, D. A.** (1996b). A revised land surface parameterization (SiB2) for atmospheric GCMs. Part II: The generation of global fields of terrestrial biophysical parameters from satellite data. *Journal of climate*, *9*(4), 706–737. https://doi.org/10.1175/1520-0442(1996)009<0706:ARLSPF>2.0.CO;2

**Sigman, D. M.**, & **Boyle, E. A.** (2000). Glacial/interglacial variations in atmospheric carbon dioxide. *Nature*, *407*(6806), 859–869. https://doi.org/10.1038/35038000

**Strassmann, K. M.**, & **Joos, F.** (2018). The Bern Simple Climate Model (BernSCM) v1. 0: An extensible and fully documented open-source re-implementation of the Bern reduced-form model for global carbon cycle–climate simulations. *Geoscientific Model Development*, *11*(5), 1887–1908. https://doi.org/10.5194/gmd-11-1887-2018

**Varney, R. M., Chadburn, S. E., Burke, E. J., Jones, S., Wiltshire, A. J.,** & **Cox, P. M.** (2023). Simulated responses of soil carbon to climate change in CMIP6 Earth system models: The role of false priming. *Biogeosciences*, *20*(18), 3767–3790. https://doi.org/10.5194/bg-20-3767-2023

**Varney, R. M., Friedlingstein, P., Chadburn, S. E., Burke, E. J.,** & **Cox, P. M.** (2024). Soil carbon-concentration and carbon-climate feedbacks in CMIP6 Earth system models. *Biogeosciences*, *21*(11), 2759–2776. https://doi.org/10.5194/bg-21-2759-2024

**Walker, A. P., De Kauwe, M. G., Bastos, A., Belmecheri, S., Georgiou, K., Keeling, R. F., McMahon, S. M., Medlyn, B. E., Moore, D. J. P., Norby, R. J., Zaehle, S., Anderson-Teixeira, K. J., Battipaglia, G., Brienen, R. J. W., Cabugao, K. G., Cailleret, M., Campbell, E., Canadell, J. G., Ciais, P., Craig, M. E., Ellsworth, D. S., Farquhar, G. D., Fatichi, S., Fisher, J. B., Frank, D. C., Graven, H., Gu, L., Haverd, V., Heilman, K., Heimann, M., Hungate, B. A., Iversen, C. M., Joos, F., Jiang, M., Keenan, T. F., Knauer, J., Körner, C., Leshyk, V. O., Leuzinger, S., Liu, Y., MacBean, N., Malhi, Y., McVicar, T. R., Penuelas, J., Pongratz, J., Powell, A. S., Riutta, T., Sabot, M. E. B., Schleucher, J., Sitch, S., Smith, W. K., Sulman, B., Taylor, B., Terrer, C., Torn, M. S., Treseder, K. K., Trugman, A. T., Trumbore, S. E., van Mantgem, P. J., Voelker, S. L., Whelan, M. E.,** & **Zuidema, P. A.** (2021). Integrating the evidence for a terrestrial carbon sink caused by increasing atmospheric $CO_2$. *New Phytologist*, *229*(5), 2413–2445. https://nph.onlinelibrary.wiley.com/doi/abs/10.1111/nph.16866

**Walker, T.**, & **Syers, J.** (1976). The fate of phosphorus during pedogenesis. *Geoderma*, *15*(1), 1–19. https://doi.org/10.1016/0016-7061(76)90066-5

**Woodward, F. I.** (1987). *Climate and plant distribution*. Cambridge University Press.

**Zhu, J., Jia, Y., Yu, G., Wang, Q., He, N., Chen, Z., He, H., Zhu, X., Li, P., Zhang, F., Liu, X., Goulding, K., Fowler, D.,** & **Vitousek, P.** (2025). Changing patterns of global nitrogen deposition driven by socio-economic development. *Nature Communications*, *16*(1), 46. https://doi.org/10.1038/s41467-024-55606-y

**TO CITE THIS ARTICLE:**

Cox, P. M., Clarke, J. J., Jones, S. R. G., & Varney, R. M. (2026). A New Method for Characterising Carbon Cycle Sensitivities in Earth System Models. *Tellus*, 79(1): 173–187. DOI: https://doi.org/10.16993/tellus.4128

**Submitted:** 28 October 2025 **Accepted:** 29 June 2026 **Published:** 03 August 2026